HHS Public Access

Author manuscript

Proc SPIE Int Soc Opt Eng. Author manuscript; available in PMC 2021 May 27.

Published in final edited form as:

Proc SPIE Int Soc Opt Eng. 2020 ; 11222: . doi:10.1117/12.2546190.

A proof-of-concept methodology to validate the *in situ* visualization of residual disease using cancer-targeted molecular agents in fluorescence-guided surgery

Servando Hernandez Vargas[1,*], **Christie Lin**[2,*], **Solmaz AghaAmiri**[1], **Julie Voss**[1], **Naruhiko Ikoma**[3], **Hop S. Tran Cao**[3], **Sukhen C. Ghosh**[1], **Adam J. Uselmann**[2], **Ali Azhdarinia**[1]

[1]Institute of Molecular Medicine, McGovern Medical School, The University of Texas Health Science Center at Houston (Houston, TX, USA)

[2]OnLume, Inc. (Madison, WI, USA)

[3]University of Texas MD Anderson Cancer Center (Houston, TX, USA)

Abstract

Introduction: The clinical need for improved intraoperative tumor visualization has led to the development of targeted contrast agents for fluorescence-guided surgery (FGS). A key characteristic of these agents is their high tumor specificity, which could enable detection of residual lesions that would likely be missed by visual inspection. Here, we examine the utility of a promising somatostatin receptor subtype-2 (SSTR2)-targeted fluorescent agent for detecting residual disease in mouse xenografts using FGS and post-operative histopathological validation.

Methods: Mice (n=2) implanted with SSTR2 overexpressing tumors were injected with 2 nmol of the dual-labeled somatostatin analog, ^{67}Ga-MMC(IR800)-TOC, and tumors were resected 48 h post-injection using traditional white light reflectance and palpation. Tumors underwent gamma counting and histopathology analysis. The wide-field FGS imaging platform (OnLume) was used to evaluate residual disease *in situ* under ambient light representative of an operating room.

Results: The tumor was resected with grossly negative margins using conventional inspection and palpation; however, additional *in situ* residual disease was found in the tumor cavity using FGS imaging. *In situ* fluorescent tumor contrast-to-noise ratios (CNRs) were 3.0 and 5.2. Agent accumulation was 7.72 and 8.20 %ID/g in tumors and 0.27 and 0.20 %ID/g in muscle. Fluorescence pixel values and gamma counts were highly correlated ($r = 0.95$, $P < 0.048$). H&E and IHC staining confirmed cancer positivity and SSTR2-overexpression, respectively.

Conclusion: Our findings demonstrate that the use of clinically relevant fluorescence imaging instrumentation enhances the evaluation of promising FGS agents for *in situ* visualization of residual disease.

Corresponding author: Ali Azhdarinia, The University of Texas Health Science Center at Houston, 1881 East Rd., 3SCR6.4680, Houston, TX 77054. Phone: 713-500-3577; Fax: 713-500-0319; ali.azhdarinia@uth.tmc.edu.

*Co-first author

Disclosures

Christie Lin and Adam J. Uselmann are employees of OnLume, Inc. The other authors declare no potential conflicts of interest.

Keywords

Cancer surgery; intraoperative imaging; fluorescence-guided surgery; fluorescence system instrumentation; targeted agent; residual disease; somatostatin receptor

Introduction:

Surgical resection is the main treatment modality for most solid cancers [1]. Advances in the surgical standard-of-care include improved diagnosis and minimally-invasive techniques that have reduced the need for radical surgeries and lead to enhanced cure rates [1]. However, a significant number of patients continue to relapse partly because of incomplete resections that result from indiscernible differences between healthy and cancer tissues [2]. The recent introduction of cancer-specific, near-infrared fluorescent (NIRF) agents into early-phase clinical trials has shown the feasibility of using targeted NIRF agents to visualize disease in the operating room [3]. The imaging technique using a fluorescent agent and fluorescence imager is known as fluorescence-guided surgery (FGS). FGS has shown the ability to provide cancer-specific contrast to enhance real-time intraoperative visualization and increase resection rates with higher specificity and sensitivity, thereby improving patient outcomes [4].

Patients with neuroendocrine tumors (NETs) are excellent candidates for FGS since (i) the only curative treatment for NETs is surgery [5, 6], (ii) 15–45% of surgical cases have incomplete resections [7–10], and (iii) surgery can still improve overall survival even in the setting of metastatic disease [6]. NETs encompass a group of poorly understood neoplasms that arise from neuroendocrine cells and predominate in the pancreas and gastrointestinal tract [11]. NETs are typically slow-growing and indolent, but ultimately lethal: nodal or liver metastases are found in 40–70% of patients at diagnosis [5] and the 5-year survival rate in metastatic patients is 19–38% [6]. Since NETs can be small (<2 cm) and highly metastatic, surgeons often have difficulty localizing NETs intraoperatively. This may lead to resections with positive or unnecessarily wide surgical margins, particularly in minimally invasive surgery where tactile feedback is absent. FGS can provide accurate tumor visualization in real time, which would enable surgeons to perform organ-sparing R0 resections that help preserve organ function and achieve superior oncological outcomes. However, the lack of intraoperative imaging agents that specifically target NETs have led to the use of non-targeted dyes, such as methylene blue or indocyanine green (ICG, the only FDA-approved NIRF dye), which offer some clinical benefit but require *high* dye doses [12, 13] that can detrimentally affect tumor-to-background contrast and may have toxicity implications [14, 15].

Radiolabeled peptides that target somatostatin receptor subtype-2 (SSTR2) have been used clinically for diagnosis, staging and preoperative planning in patients with NETs for over 30 years [16–18]. Unfortunately, preoperative imaging only locates the amount and extent of disease, but does not provide surgeons with *in situ* disease visualization for detection of surgical margins and post-resection residual disease. In response, our group developed a chemistry scaffold that expands the utility of the clinical approved SSTR2-targeted

radiotracer,^{68}Ga-DOTA-TOC, into a fluorescently-labeled analog. Using a multimodality chelator (MMC) as a "radioactive" linker, we conjugated the NIRF dye, IRDye800 (IR800), to produce ^{68}Ga-MMC(IR800)-TOC with intact pharmacological properties [19] and high specificity to the human receptor somatostatin receptor subtype-2 (SSTR2) [20].

It is widely accepted that the clinical adoption of NIRF FGS would significantly benefit from (i) the ability to perform real-time intraoperative NIRF visualization under ambient light and (ii) identification of an optimized drug-device pairing [21, 22]. Additionally, established methods for validating the performance of tumor-specific NIRF agents and drug-device combinations are currently lacking [23]. Here, we seek to address these issues in a proof-of-concept study for the *in situ* visualization of residual disease with a wide-field FGS imaging platform that is designed for clinical use. The custom benchtop FGS imaging platform (OnLume, Madison, WI) was designed to optimally image ^{68}Ga-MMC(IR800)-TOC under conventional operating room lighting conditions. Finally, we cross-validate and demonstrate the potential added value of targeted FGS for subclinical, residual disease detection *in situ.*

Methods:

Radiolabeling MMC(IR800)-TOC with ^{67}Ga

MMC(IR800)-TOC was radiolabeled with ^{67}Ga ($t_{1/2}$ = 78 hours) using cation exchange chromatography to enable delayed quantification as previously described [20].

Cell culture and animal model

SSTR2-overexpressing HCT116 (HCT116-SSTR2) cells were cultured as previously described [20]. Athymic female nu/nu mice (Charles River Laboratories) (n = 2) were housed under standards of the Institutional Animal Care and Use Committee (IACUC) of the University of Texas Health Science Center at Houston and maintained on alfalfa-free rodent chow. For all procedures mice were anesthetized with 1% to 2% isoflurane. Mice were subcutaneously implanted with 6×10^6 HCT116-SSTR2 cells in Matrigel (Corning):PBS (1:1) in the shoulder and implants were grown for two weeks. Studies were terminal and overdose of anesthesia followed by cervical dislocation was the method of euthanasia.

In vitro optimization of FGS imaging platform to MMC(IR800)-TOC

A wide-field benchtop imaging platform was customized for optimal MMC(IR800)-TOC contrast-to-noise ratio (CNR) imaging. The FGS imaging platform includes onboard white light illumination, NIRF excitation sources, and simultaneous white light reflectance and fluorescence imagers (OnLume, Inc). Several excitation and emission filter sets were tested to control the desired fluorescence that reaches the imager and determine optimal image contrast and sensitivity. To achieve this, two-fold serial dilutions of MMC(IR800)-TOC in deionized water were prepared *in vitro* and images were acquired.

Mimicking standard surgical procedures followed by *in situ* fluorescence imaging

Mice were intravenously injected with 2 nmol of ^{67}Ga-MMC(IR800)-TOC 48 hours prior to tumor resection. All procedures were performed under white light reflectance surgical field

illumination with bright ambient light conditions representative of a standard-of-care surgery. Surgical removal of gross tumor masses were performed using only direct visual inspection and palpation. Following final inspection of the tumor bed, fluorescence imaging was performed on the surgical site. The tumor bed was inspected using fluorescence on white light overlay provided on the platform's real-time video display. Sources of ambient light, such as overhead room lights, were not modified. The resected gross tumor was placed in the wound bed alongside residual disease, if any, and imaged *in situ* using both white light and fluorescence imaging. For this proof-of-concept study, any fluorescent tissue was resected under the suspicion of being residual disease.

All images were captured in triplicates and the average and standard deviation of each were recorded. CNRs of regions-of-interest (ROIs) were calculated as:

$$CNR = (S_R - S_b)/\sigma_b \quad (1)$$

where S_R is the fluorescent signal in the ROI, S_b is the fluorescent signal in the background tissue (i.e., muscle), and σ_b is the standard deviation of fluorescent signal in background tissue.

Biodistribution

At the conclusion of the imaging study, resected tissues underwent gamma counting in a Wizard^2 gamma counter (Perkin Elmer) and percent injected dose per gram of tissue (%ID/g) was calculated. The total injected activity per mouse was determined from a known aliquot of the injected solution.

Histopathology

Suspected residual disease and muscle tissue from each mouse were cryo-conserved in optimal cutting temperature (OCT) compound and used to prepare frozen sections (thickness = 5 μm). Hematoxylin & eosin (H&E) and Immunohistochemistry (IHC) staining of frozen sections were prepared to permit morphological analysis of tissues and to identify SSTR2 expression, respectively, as previously described [20].

Statistical analysis

Graphing and statistical analysis was performed with GraphPad Prism 8.1.0. The Pearson correlation coefficient (r) was calculated assuming data are sampled from Gaussian distribution. Significance level was set to $P < 0.05$ (two-tailed). All data are presented as mean ± standard deviation (SD).

Results:

Two-fold serial dilutions of MMC(IR800)-T0C were prepared *in vitro* (molarity range: 3 to 1×10^5 nM) and imaged at a working distance of 39 cm between the imager and the surface of the ROI. The full dilution series was imaged in a single field-of-view (Fig. 1A). Imaging acquisition Set C was selected for the proof-of-concept study due to its consistently higher CNR as compared to the other two filter sets (Fig. 1B).

In situ NIRF imaging was performed prior to tumor resection and CNRs of the gross tumors for mouse 1 (M1) and mouse 2 (M2) were 3.0 and 5.2, respectively. Standard-of-care surgical removal of gross tumor masses was then conducted until achieving 'negative' margins and white light images were captured (Fig. 2A and 2C). Standard-of-care surgical techniques were defined in this study as direct visual inspection under white light reflectance and palpation.

Subsequently, FGS imaging was performed using the imaging platform (OnLume) to evaluate residual fluorescence *in situ* under bright ambient light conditions. Inspection of the tumor bed using real-time video of fluorescence overlay on white light reflectance demonstrated the presence of residual fluorescence in the tumor cavity of both mice (Fig. 2B and 2D). *In situ* CNRs of residual fluorescence were 2.6 and 4.2 for M1 and M2, respectively.

^{67}Ga-MMC(IR800)-TOC accumulation was 7.72 (M1) and 8.20 (M2) %ID/g in tumors and 0.27 (M1) and 0.20 (M2) %ID/g in muscle. Fluorescence pixel values and gamma counts were highly correlated for tumor and muscle tissue ($r = 0.95$, $P < 0.048$) (Fig. 3).

Histopathological analysis of suspected residual disease using H&E and IHC staining confirmed cancer positivity and SSTR2-overexpression, respectively (Fig. 4).

Discussion:

Tumor-associated biomarkers (i.e., cell surface receptors and antigens) have long been exploited as targets for cancer detection by diagnostic imaging techniques [24–27]. SSTR2 has played a central role in the advancement of diagnostic imaging agents and is the foundation of the most well characterized nuclear imaging platform in cancer, making it an ideal target for development of an FGS counterpart. We previously used a custom synthesis strategy to conjugate a NIRF dye to ^{68}Ga-DOTA-TOC, and showed remarkable retention of receptor specificity in cells and animal models. In order to determine if preclinical findings with the resulting FGS agent, MMC(IR800)-T0C, could translate into clinical benefit to patients with NETs, further evaluation of imaging performance was done using a novel FGS imager equipped with clinical-grade optics, electronics, and software. Customization of an imaging device to the fluorescent agent may enhance detection sensitivity, and further improve tumor delineation [21]. Most clinical FGS imagers are designed to be compatible with ICG, which has significantly different excitation and emission spectra from IR800, hindering performance when used with this dye [24]. For this reason, the wide-field FGS benchtop imaging platform was initially evaluated on *in vitro* serial dilutions of MMC(IR800)-T0C to optimize its sensitivity and image contrast. Optimization of the optical components of the device with respect to the excitation and emission spectra of the drug lead to characterization of low drug concentrations, which could conceivably enable the use of microdoses (i.e., sub-pharmacologic) in patients and offer the corresponding advantages of higher contrast, reduced toxicity, and lower cost [28, 29].

Ideally, preclinical imaging studies would be performed under conditions that closely resemble the clinical setting in order to identify translational barriers in FGS agent

development. However, clinical FGS imaging systems are not typically used during preclinical research, and preclinical imaging devices have key differences in their optical specifications that hinder the assessment of translational feasibility. This includes (i) lower sensitivity that limits microdose detection, (ii) long exposure times that lack real-time functionality, and (iii) control of known factors that degrade image quality (i.e., ambient light). The presence of ambient light in the operating room is particularly significant since it can contaminate the fluorescence signal captured by the imager and provide inferior image quality. For several commercial imagers that are used in open surgery, the instructions for use require setting room light levels to 'low' or 'off' [30]. Our objective was to design an imaging system that can effectively obtain high quality images regardless of lighting conditions, and exhibit minimal impact on how standard-of-care surgery is performed. As shown in the *in vivo* studies, ambient overhead fluorescent tube lights were 'on' to enable full illumination intensity but did not impair the ability of the imager to clearly identify gross tumors and microlesions with high contrast.

The clinical impact of an FGS imaging platform depends upon the collective properties of the drug and device to detect contrast-enhanced target tissues with high sensitivity. This capability is especially critical in small or dimly fluorescent regions (i.e., tumor margins or sites of residual disease) such that imaging provides a true positive readout rather than a false negative that may occur with visual cues alone. The presence of any cancerous cells left following surgical resection could potentially result in tumor recurrence and poor clinical outcomes. We showed that the excellent tumor-targeting properties of MMC(IR800)-TOC enabled visualization of residual disease above fluorescent signal noise, which is the sum of autofluorescence, scattering, leakage due to reflection, and the camera sensor's inherent noise. Despite the small size of the microlesions and low amount of drug present, the excellent sensitivity of the imager allowed malignant residues to be detected with sufficient contrast [31] and produced intraoperative images that could conceivably aid surgeons in identifying residual cancer in tumor margins, cancer-positive lymph nodes, and locoregional metastases that are often present in patients with NETs [5, 6]. Similar methods could also be applied in cancers that possess promising tumor-targeting compounds, such as the use of small molecules that target prostate-specific membrane antigen (PSMA) in prostate cancer, in order to extend the benefits of FGS to broad patient populations. The modular design of the MMC could readily be incorporated into PSMA-targeted radiotracers to develop a fluorescent analog, and optimization of the imager would ensure maximum efficiency in detecting fluorescence signals emitted from novel FGS agents.

Conclusion:

Our findings demonstrate that the use of preclinical fluorescence imaging instrumentation designed with clinically relevant imaging attributes enhances the *in vivo* visualization of residual disease. *In situ* fluorescence (intraoperative measurement) was validated against its absolute gamma counts as well as H&E and IHC analysis (post-operative pathology) to confirm the presence of residual disease in the tumor bed. Through the use of a customized drug-device combination, we show the feasibility of detecting sub-clinical, residual disease in SSTR2-expressing tumors.

References

1. Wyld L, Audisio RA, and Poston GJ, The evolution of cancer surgery and future perspectives. Nat Rev Clin Oncol, 2015. 12(2): p. 115–24. [PubMed: 25384943]
2. Orosco RK, et al., Positive Surgical Margins in the 10 Most Common Solid Cancers. Sci Rep, 2018. 8(1): p. 5686. [PubMed: 29632347]
3. Hernot S, et al., Latest developments in molecular tracers for fluorescence image-guided cancer surgery. The Lancet Oncology, 2019. 20(7): p. e354–e367. [PubMed: 31267970]
4. Tipirneni KE, et al., Oncologic Procedures Amenable to Fluorescence-guided Surgery. Ann Surg, 2017. 266(1): p. 36–47. [PubMed: 28045715]
5. Ramage JK, et al., Guidelines for the management of gastroenteropancreatic neuroendocrine (including carcinoid) tumours (NETs). Gut, 2012. 61(1): p. 6–32. [PubMed: 22052063]
6. Wang R, et al., Management of Gastrointestinal Neuroendocrine Tumors. Clin Med Insights Endocrinol Diabetes, 2019. 12: p. 1179551419884058.
7. Landerholm K, et al., Survival and prognostic factors in patients with small bowel carcinoid tumour. Br J Surg, 2011. 98(11): p. 1617–24. [PubMed: 21858790]
8. Bosch F, et al., Surgical treatment of pNET - Experience of a “high-volume” center. Surg Oncol, 2018. 27(3): p. 409–414. [PubMed: 30217295]
9. Dasari BVM, et al., Outcomes of Surgical and Endoscopic Resection of Duodenal Neuroendocrine Tumours (NETs): a Systematic Review of the Literature. J Gastrointest Surg, 2018. 22(9): p. 1652–1658. [PubMed: 29869091]
10. Yang M, et al., Survivals of patients with surgically treated and High-grade pancreatic neuroendocrine carcinomas: A comparative study between two American Joint Committee on Cancer 8th tumor-node-metastasis staging systems. Eur J Surg Oncol, 2019. 45(6): p. 1054–1060. [PubMed: 30661921]
11. Chauhan A, Kohn E, and Del Rivero J, Neuroendocrine Tumors-Less Well Known, Often Misunderstood, and Rapidly Growing in Incidence. JAMA Oncol, 2019.
12. Paiella S, et al., Is there a role for near-infrared technology in laparoscopic resection of pancreatic neuroendocrine tumors? Results of the COLPAN “colour-and-resect the pancreas” study. Surg Endosc, 2017. 31(11): p. 4478–4484. [PubMed: 28374260]
13. Handgraaf HJM, et al., Intraoperative Near-Infrared Fluorescence Imaging of Multiple Pancreatic Neuroendocrine Tumors: A Case Report. Pancreas, 2018. 47(1): p. 130–133. [PubMed: 29232342]
14. Ginimuge PR and Jyothi SD, Methylene Blue-Revisited. J Anaesth Clin Pharmacol, 2010. 26(4): p. 517–520.
15. Nagaya T, et al., Fluorescence-Guided Surgery. Front Oncol, 2017. 7: p. 314. [PubMed: 29312886]
16. Krenning EP, et al., Localisation of endocrine-related tumours with radioiodinated analogue of somatostatin. Lancet Lond. Engl, 1989. 1: p. 242–244.
17. Hofmann M, et al., Biokinetics and imaging with the somatostatin receptor PET radioligand (68)Ga-DOTATOC: preliminary data. Eur J Nucl Med, 2001. 28(12): p. 1751–7. [PubMed: 11734911]
18. Frilling A, et al., The impact of 68Ga-DOTATOC positron emission tomography/computed tomography on the multimodal management of patients with neuroendocrine tumors. Ann Surg, 2010. 252(5): p. 850–6. [PubMed: 21037441]
19. Ghosh SC, et al., Synthesis of a Fluorescently Labeled (68)Ga-DOTA-TOC Analog for Somatostatin Receptor Targeting. ACS Med Chem Lett, 2017. 8(7): p. 720–725. [PubMed: 28740605]
20. Hernandez Vargas S, et al., Specific Targeting of Somatostatin Receptor Subtype-2 for Fluorescence-Guided Surgery. Clin Cancer Res, 2019. 25(14): p. 4332–4342. [PubMed: 31015345]
21. Rosenthal EL, et al., Successful Translation of Fluorescence Navigation During Oncologic Surgery: A Consensus Report. J Nucl Med, 2016. 57(1): p. 144–50. [PubMed: 26449839]
22. Tummers WS, et al., Regulatory Aspects of Optical Methods and Exogenous Targets for Cancer Detection. Cancer Res, 2017. 77(9): p. 2197–2206. [PubMed: 28428283]

23. Pogue BW, et al., Perspective review of what is needed for molecular-specific fluorescence-guided surgery. J Biomed Opt, 2018. 23(10): p. 1–9.

24. Smith CJ, Volkert WA, and Hoffman TJ, Radiolabeled peptide conjugates for targeting of the bombesin receptor superfamily subtypes. Nucl Med Biol, 2005. 32(7): p. 733–40. [PubMed: 16243649]

25. Huang L, et al., SPECT imaging with 99mTc-labeled EGFR-specific nanobody for in vivo monitoring of EGFR expression. Mol Imaging Biol, 2008. 10(3): p. 167–75. [PubMed: 18297364]

26. Dijkers EC, et al., Biodistribution of 89Zr-trastuzumab and PET imaging of HER2-positive lesions in patients with metastatic breast cancer. Clin Pharmacol Ther, 2010. 87(5): p. 586–92. [PubMed: 20357763]

27. Afshar-Oromieh A, et al., The diagnostic value of PET/CT imaging with the (68)Ga-labelled PSMA ligand HBED-CC in the diagnosis of recurrent prostate cancer. Eur J Nucl Med Mol Imaging, 2015. 42(2): p. 197–209. [PubMed: 25411132]

28. Pogue BW, et al., Advancing Molecular-Guided Surgery through probe development and testing in a moderate cost evaluation pipeline. Proc SPIE Int Soc Opt Eng, 2015. 9311.

29. Burt T, et al., Microdosing and Other Phase 0 Clinical Trials: Facilitating Translation in Drug Development. Clin Transl Sci, 2016. 9(2): p. 74–88. [PubMed: 26918865]

30. AV DS, et al., Review of fluorescence guided surgery systems: identification of key performance capabilities beyond indocyanine green imaging. J Biomed Opt, 2016. 21(8): p. 80901. [PubMed: 27533438]

31. Hoogstins C, et al., Setting Standards for Reporting and Quantification in Fluorescence-Guided Surgery. Mol Imaging Biol, 2019. 21(1): p. 11–18. [PubMed: 29845427]

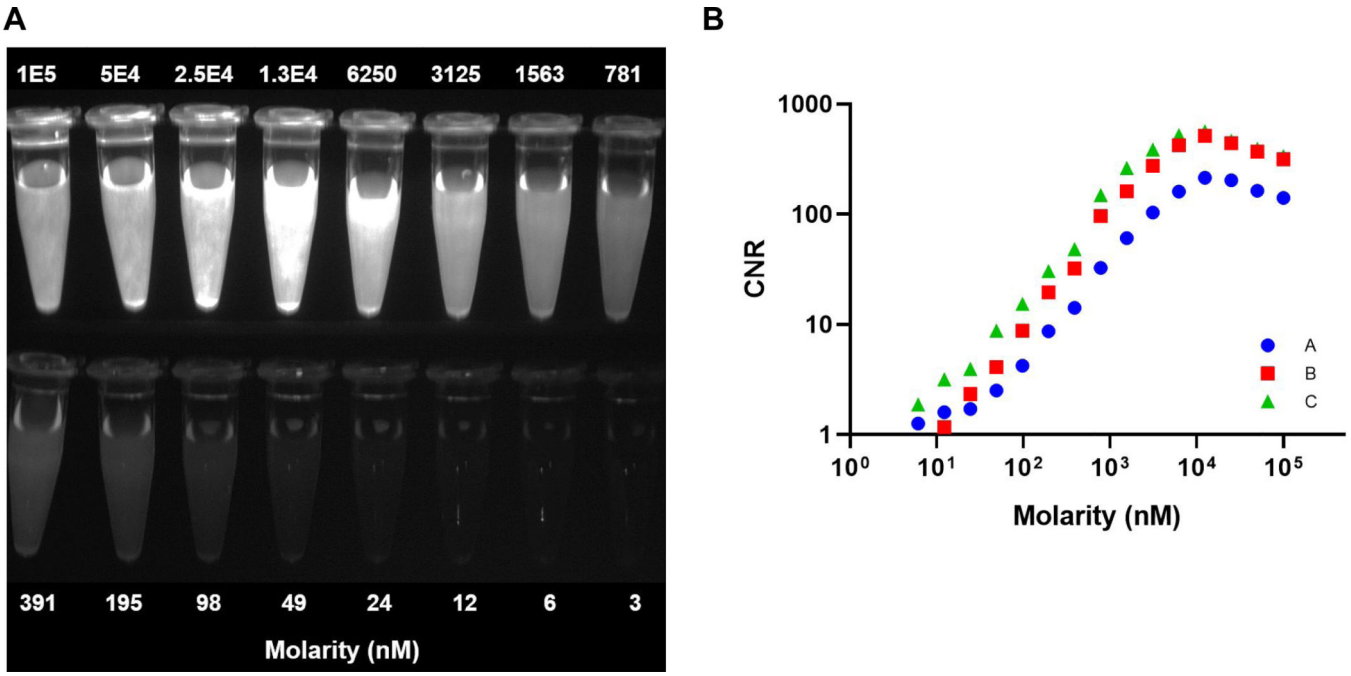

Figure 1. ***In vitro*** **imaging of MMC(IR800)-TOC for contrast optimization.**

(A) Fluorescence-only image of two-fold MMC(IR800)-TOC serial dilutions. Only Set C is shown. **(B)** Contrast-to-noise ratio (CNR) of the molarity of MMC(IR800)-TOC, measured with three different excitation and emission filter sets (Sets: A = ●, B = ■, and C = ▲).

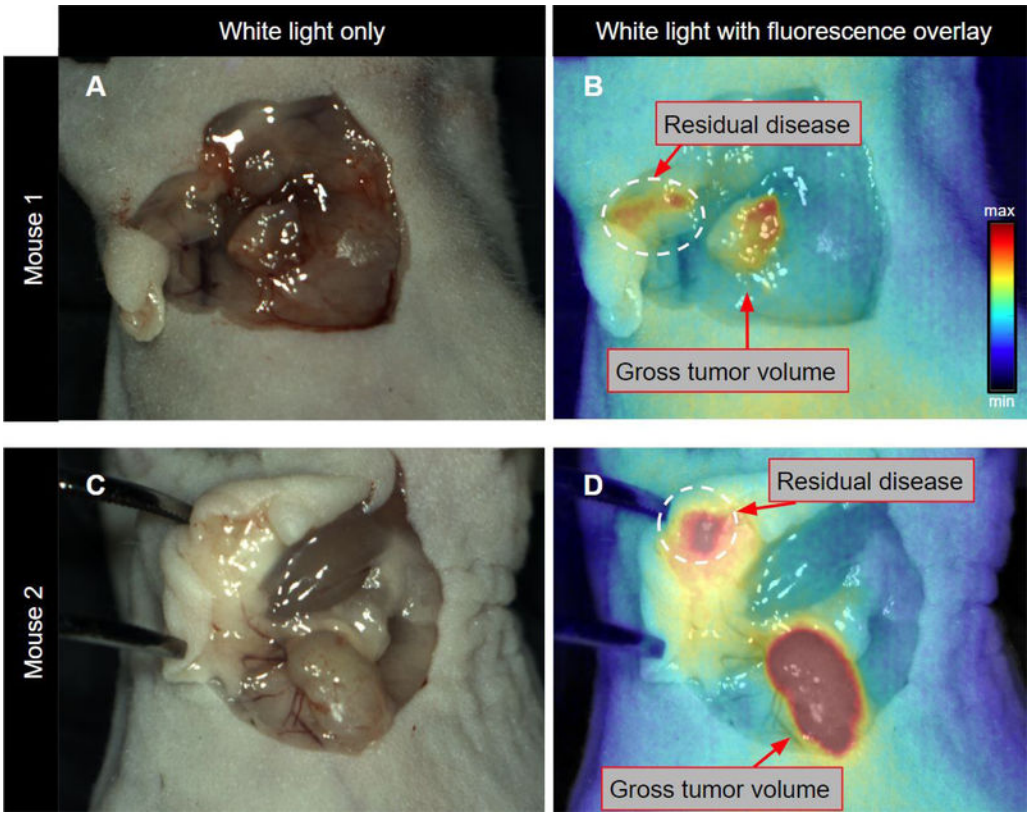

Figure 2. Intraoperative visualization of residual disease following gross tumor resection under ambient light.

White light *in situ* visualization after tumor resection using direct visual inspection and palpation only (for the proof-of-concept study tumors were placed back in the field of view) (**A** and **C**). Tumor beds were then surveyed using the OnLume FGS imaging system and residual fluorescence was detected (circumscribed by dashed white circle) (**B** and **D**). **B** and **D** are the corresponding NIRF images overlaid on A and B, respectively.

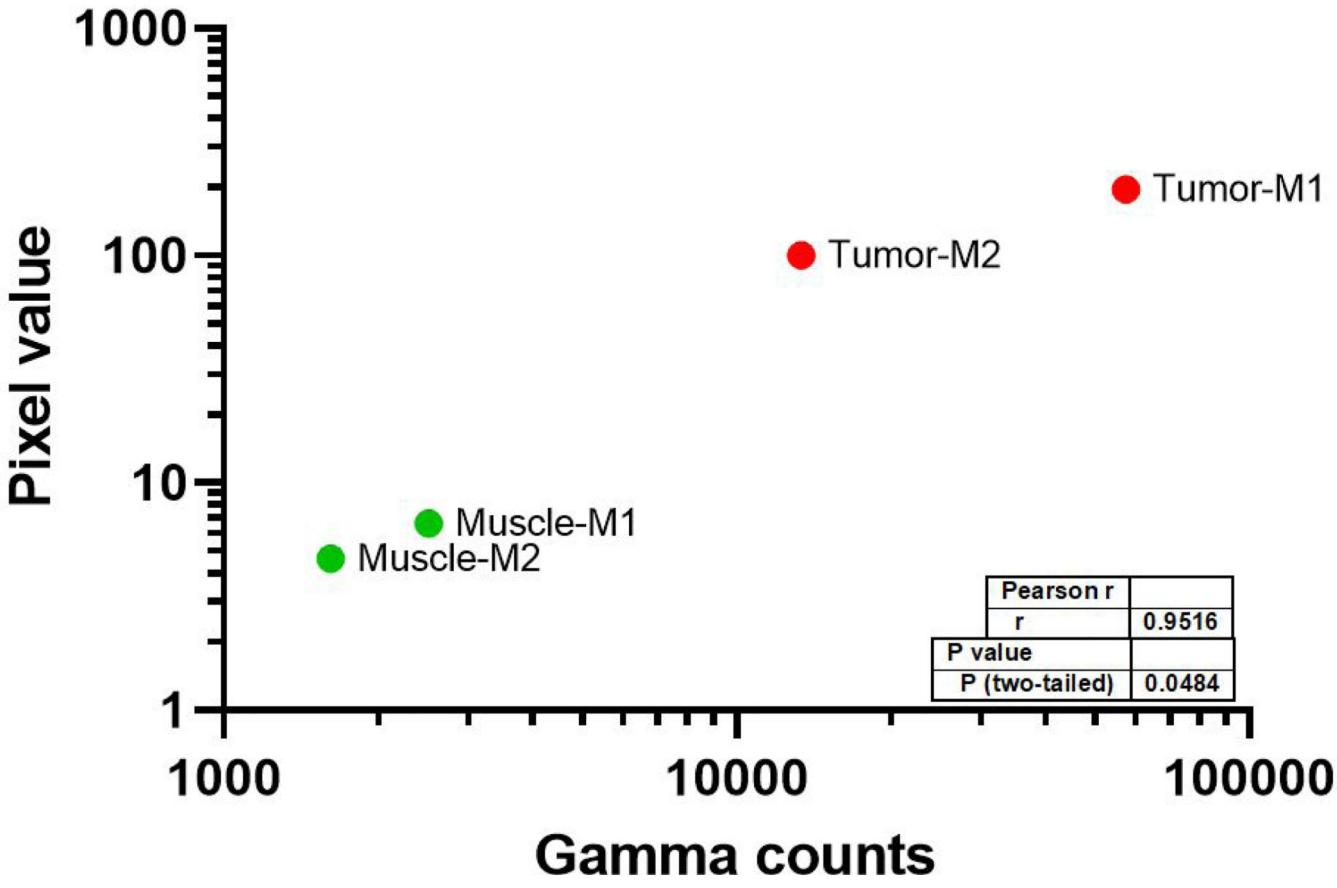

Figure 3. Relationship between the fluorescence acquired by the FGS system and the absolute delivered dose of ^{67}Ga-MMC(IR800)-TOC.

In situ fluorescent pixel values captured by the OnLume FGS imaging system were cross-validated and correlated to the gamma counts of ^{67}Ga-MMC(IR800)-TOC. The gamma counts enable accurate quantification of ^{67}Ga-MMC(IR800)-TOC accumulation independent of fluorescence output and imaging device. M1 = Mouse 1; M2 = Mouse 2.

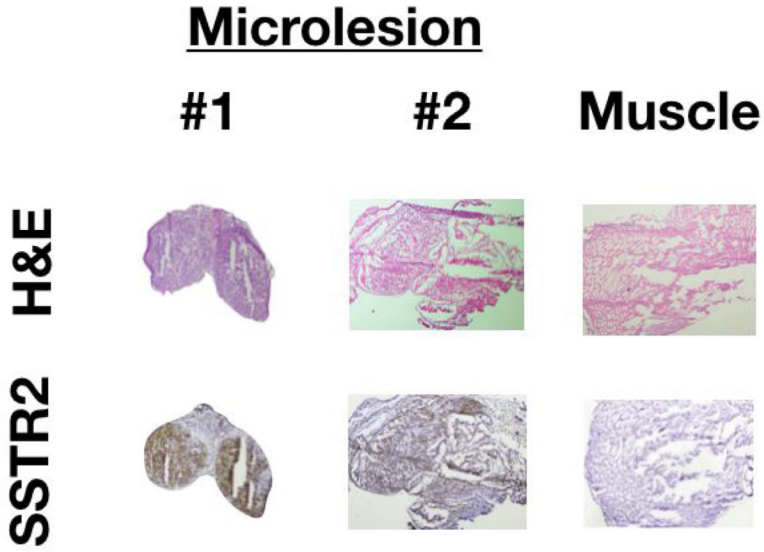

Figure 4. Histological analysis of residual fluorescence was confirmed for cancer positivity and SSTR2-overexpression.

The top row shows H&E staining for tumor and muscle (n = 2). The bottom row shows corresponding IHC staining, which indicates SSTR2 presence only in tumors (malignant cells: brown areas).